Geophysical Research Letters

RESEARCH LETTER
10.1029/2023GL106201

Crustal Heterogeneity of Antarctica Signals Spatially Variable Radiogenic Heat Production

L. Li[1] and A. R. A. Aitken[1,2]

[1]School of Earth Sciences, The University of Western Australia, Perth, WA, Australia, [2]Australian Centre of Excellence for Antarctic Science, The University of Western Australia, Perth, WA, Australia

Key Points:

- A new Antarctic crustal model is derived by seismic-constrained gravity inversion
- Variations in crustal radiogenic heat production are inferred from upper-crust density and geochemical data
- The potential impact of heterogeneity in crustal heat production for geothermal heat flow is quantified

Supporting Information:

Supporting Information may be found in the online version of this article.

Correspondence to:

L. Li,
lu.li@uwa.edu.au

Citation:

Li, L., & Aitken, A. R. A. (2024). Crustal heterogeneity of Antarctica signals spatially variable radiogenic heat production. *Geophysical Research Letters*, *51*, e2023GL106201. https://doi.org/10.1029/2023GL106201

Received 1 SEP 2023
Accepted 7 JAN 2024

Author Contributions:

Conceptualization: L. Li, A. R. A. Aitken
Data curation: L. Li
Formal analysis: L. Li
Funding acquisition: A. R. A. Aitken
Investigation: L. Li, A. R. A. Aitken
Methodology: L. Li, A. R. A. Aitken
Project Administration: L. Li, A. R. A. Aitken
Resources: L. Li
Software: L. Li
Supervision: A. R. A. Aitken
Validation: L. Li, A. R. A. Aitken
Visualization: L. Li
Writing – original draft: L. Li
Writing – review & editing: L. Li, A. R. A. Aitken

Abstract Geothermal heat flow (GHF) is a key basal boundary condition for Antarctic ice-sheet flow. Large-scale variations are resolved by several recent models but knowledge of the smaller-scale variations, crucial for ice sheet dynamics, is limited by unresolved variations in crustal radiogenic heat production. To define this at continent-scale we use 3D gravity inversion constrained by seismic Moho estimates to identify variations in crustal composition and geometry beneath thick ice. Geochemically-defined empirical relationships between density and heat production capture the global average trend and its variability, and allow to estimate from upper-crust density spatial variations in radiogenic heat production. Significant variations are observed typically 1.2–1.6 $\mu W/m^3$, and as high as 2 $\mu W/m^3$ in West Antarctica. The contribution to GHF from these heat-production variations is similarly variable, typically 16–24 mW/m^2 and up to 60 mW/m^2. The mapped variations are significant for correctly representing GHF in Antarctica.

Plain Language Summary Antarctica's crustal structure - including sedimentary basins, the igneous and metamorphic crust, and the interface between the crust and mantle - dictates the delivery of heat from depth to the ice sheet's base, with capacity to influence ice sheet flow. Crustal structure is not well-understood due to the extensive and thick ice cover combined with limited geophysical observations. We investigate the variations in crustal geometry and density, by examining anomalies in the Earth's gravity field and using independent depth constraints from seismic studies. Our findings indicate substantial variations in heat production characterized by heterogeneous crustal structure, influencing the heating of the ice sheet's base to a significant degree.

1. Introduction

To make accurate predictions of future changes of Antarctic ice-sheet, it's essential to understand the subglacial boundary conditions, particularly geothermal heat flow (GHF). GHF is an important factor in controlling the basal thermal state and ice rheology (Noble et al., 2020). Areas with a thawed bed generate basal melting water and contribute to subglacial hydrology (McCormack et al., 2022), which is a known factor driving ice sheet dynamics (Bell, 2008). Even in areas with a frozen-bed, GHF impacts basal temperature, which determines the extent of deformation processes occurring within the ice-sheet (Hooke, 2019).

Due to the inaccessibility of the ice-sheet bed, there are limited direct observations of GHF, and large-scale understanding relies heavily on models derived from geophysical data (Burton-Johnson et al., 2020; Reading et al., 2022). Spatially variable GHF for Antarctica has been estimated in the past using magnetic (Martos et al., 2017) and seismic methods (An et al., 2015b; Haeger et al., 2022; Hazzard et al., 2023). These methods characterize the thermal structure of the lithosphere by the geometry of the inferred Curie isotherm (Martos et al., 2017) or the temperature field of the lithospheric mantle (An et al., 2015b; Haeger et al., 2022; Hazzard et al., 2023). GHF is then calculated from the thermal gradient between the isotherm and the ice-sheet bed. In the absence of a knowledge of crustal properties, the thermal-gradient calculation relies on assumed thermal properties, often held constant, which may fail to represent well the reality. Some recent GHF models can account for crustal heterogeneity by using statistical methods with multivariate-geophysical data (Lösing & Ebbing, 2021; Stål et al., 2021). These models consistently represent GHF variation over long-length scales (>300 km wavelength). Still, the models often diverge on a smaller scale due to differences in the methods used (Reading et al., 2022).

A challenge of current models is the limited knowledge and resolution available when accounting for the effects of variable crustal radiogenic heat production, which can account for 26%–40% of total heat flow (Hasterok &

Chapman, 2007, 2011), and may vary significantly on small length-scales. Interpolations derived from large-scale models from univariate data will fail to represent local variations, and yet these are critical for controlling ice-sheet dynamics (McCormack et al., 2022; Reading et al., 2022). Therefore, a way forward is to generate high-resolution crustal models that can capture the variations in crustal properties and structure. Such models could then be used to understand GHF variations using forward or statistical approaches (Lösing et al., 2020).

In Antarctica, both seismic and gravity applications resolve substantial regional variations in crust and mantle structure (Abrehdary & Sjöberg, 2021; Haeger & Kaban, 2019; Haeger et al., 2019; Lloyd et al., 2020; Pappa et al., 2019a, 2019b; Stål et al., 2019). Studies of Antarctic crustal structure have mainly focused on the interface between crust and mantle (marked by Moho discontinuity). This interface is primarily constrained by receiver function analysis (Baranov & Morelli, 2013; Chaput et al., 2014; Dunham et al., 2020; Hansen et al., 2009). Recent applications have also begun to resolve structure within the crust (Zhou et al., 2022). However, due to the challenging fieldwork environment, seismic observations are sparse and have uneven spatial coverage, which limits their ability to resolve crustal structures in detail.

Benefiting from the more consistent spatial coverage of airborne and satellite gravity measurement, gravity inversion is an alternative approach to estimate the Moho undulations, variably constrained by seismic information (Chisenga et al., 2019; Llubes et al., 2018; Pappa et al., 2019a; Zhang et al., 2020). These studies assume that long-wavelength Bouguer gravity reflects Moho undulations and use geometry inversion techniques with a single density contrast to recover the Moho. However, this assumption is problematic in continental-scale applications due to lateral variations in crust and mantle density structure that can generate gravity anomalies of comparable magnitude to the Moho as well as affecting density contrast across the interface (Aitken, 2010; Aitken et al., 2013). An additional challenge is raised due to the large uncertainties in the topography and ice thickness data in Antarctica (Morlighem et al., 2020), which would directly impact the resolved Bouguer gravity. Free-air gravity is unaffected by this uncertainty, although there is still a requirement for topographic gravity effects to be modeled.

An alternative approach involves incorporating all critical surfaces and density structures as updatable features within a single model domain. A 3D gravity inversion is then utilized to optimize the density and surface geometries to fit the gravity data (Aitken, 2010; Aitken et al., 2013; Alghamdi et al., 2018). This approach accounts for a laterally heterogeneous crust and mantle with the capability to generate seismic-constrained Moho and density structure in a continental-scale application (Aitken, 2010; Aitken et al., 2013).

Here, we build a 3D model domain including sedimentary basin, upper and lower crust layers and mantle. During the inversion, the density and thickness of each layer are modified within seismic constraints and density bounds, and with differing constraints applied to the solution. An ensemble of results is assembled that fits both the gravity observations and the prior seismic constraints. The ensemble result presents the most representative model of Antarctic crustal structure possible within the capacity of the method and current data constraints. From the ensemble result and empirical relationships between density and radiogenic heat production from a global geochemical database, we explore the implications of heterogeneity in crustal composition and structure for radiogenic heat production and GHF in Antarctica.

2. Data and Methods

2.1. Free-Air Gravity Data and Initial Model

In our inversion, we invert free-air gravity data. For the data set, airborne gravity data sets (the AntGG compilation (Scheinert et al., 2016) and regional-scale free-air gravity data, Text S1 in Supporting Information S1) are combined with the GOCO06s satellite gravity model (Kvas et al., 2019) calculated at 5 km ellipsoid height (Figure S1 in Supporting Information S1). After merging, the long-wavelength gravity information predominantly caused by the mantle convection or sub-lithospheric mantle density variations was removed using the spherical harmonics 0–10° (>2,000 km half-wavelength) from GOCO06s model.

The initial model incorporates the current understanding of Antarctic crustal structure, with a horizontal grid resolution of 20 km and extending to a depth of 75 km. It is divided into nine layers, including ice, lake water, seawater, sedimentary basins (with three layers accounting for sediment compaction with depth), crystalline crust (upper and lower crust), and mantle (Text S2 in Supporting Information S1). The topographic components of the

model are represented by BedMachine Antarctica (Morlighem et al., 2020). Initial sedimentary basin thickness is scaled from the relationship between sedimentary basin distribution likelihood model (Li et al., 2022) with thickness from individual estimations (Text S3 in Supporting Information S1). Initial Moho surface and its uncertainty are based on the kriging prediction and error using individual Moho estimates (see An et al. (2015a) and Table S2 in Supporting Information S1). The prediction error from kriging is used to represent the bounds of permissible Moho surface (±2 standard deviation). Within the crust, a two-layer equal thickness upper and lower crust is used in the continental crust to provide essential density contrasts at surface and Moho and a single-layer crust is used in the oceanic crust. The initial and permitted density ranges for each layer are shown in Table S1 in Supporting Information S1.

2.2. Gravity Inversion

3D gravity inversions were undertaken using VPMG software (Fullagar et al., 2008), which divides the model domain with prism-elements of pre-defined area but with arbitrary thickness. VPMG has two main gravity inversion styles: density-style, where the densities of prism-elements are varied, and geometry-style, where the elevations of the prism-element boundaries are modified. Each style works independently, and the other property cannot change.

This study followed the alternating inversion method used by Aitken et al. (2013), Alghamdi et al. (2018), and Moro et al. (2023). Each of our model runs ran three cycles of four single-iteration inversions, respectively one iteration for mantle density, then one iteration each for the density within the crust layers, the geometry of the Moho, and the sedimentary basin thickness. The overall inversion process is regulated by the maximum permitted change in each style: for a density inversion, the permitted change is the maximum density change in the current iteration; for a geometry style inversion, the permitted change is set as the maximum percentage of the interface elevation change. Increasing permitted changes allows more change to be accommodated in that phase, which increases the potential to resolve misfit through that style of inversion.

In total 35 inversions were run to generate a model-ensemble each containing results constrained by different permitted density or geometry changes. The permitted density change ranged from 5 kg/m^3 to 40 kg/m^3 by 5 kg/m^3 intervals while geometry change ranged from 5% to 13% by 2% intervals (Figure S5 in Supporting Information S1). Six models that do not sufficiently converge with gravity observation (misfit >10 mGal) are rejected and excluded from the model-ensemble. We use the mean of the model-ensemble and its standard deviation to show a representative crustal structure (Text S4 in Supporting Information S1).

2.3. Estimating Radiogenic Heat Production

For mapping of density to heat production, we estimate the statistical relationship between rock density and heat production computed from the global whole-rock geochemical database (Gard et al., 2019a) (Figures 1a and 1b, Text S6 in Supporting Information S1). For the global database, there is a large-scale trend that heat production decreases with increasing density value, albeit with non-linear behavior at the tails. It is clear from the scatter plot (Figure 1a) that the correlation between heat production and density is generally weak due to large natural variability between samples, which has been well documented in previous studies (e.g., heat production vs. silica content (Gard et al., 2019b), heat production versus Vp or density (Hasterok & Webb, 2017)). Despite the absence of a physically-based model to link heat production with density, the consistency between average density and heat production values across continents suggests a robust predictive power in using this empirical relationship (Hasterok & Webb, 2017).

It is of note that our geophysical model elements comprise prisms with areas of 400 km^2 and several kilometers to tens of kilometers thick. This volume comprises a mixture of lithologies and compositions, including variable proportions of mafic, felsic and intermediate composition rocks, as well as trace amounts of dense minerals such as garnet, olivine and iron oxides. The natural variations in heat production for individual rocks and lithologies will be mitigated by the very large volume sampled; we will detect in our model only systematic trends in the composition of rocks and factors such as metamorphic grade, that are also well represented in the geochemical database.

Although we cannot precisely estimate a heat production value from density for individual samples, the global median heat production and density are strongly correlated in density range between 2,650 and 2,950 kg/m^{-3}

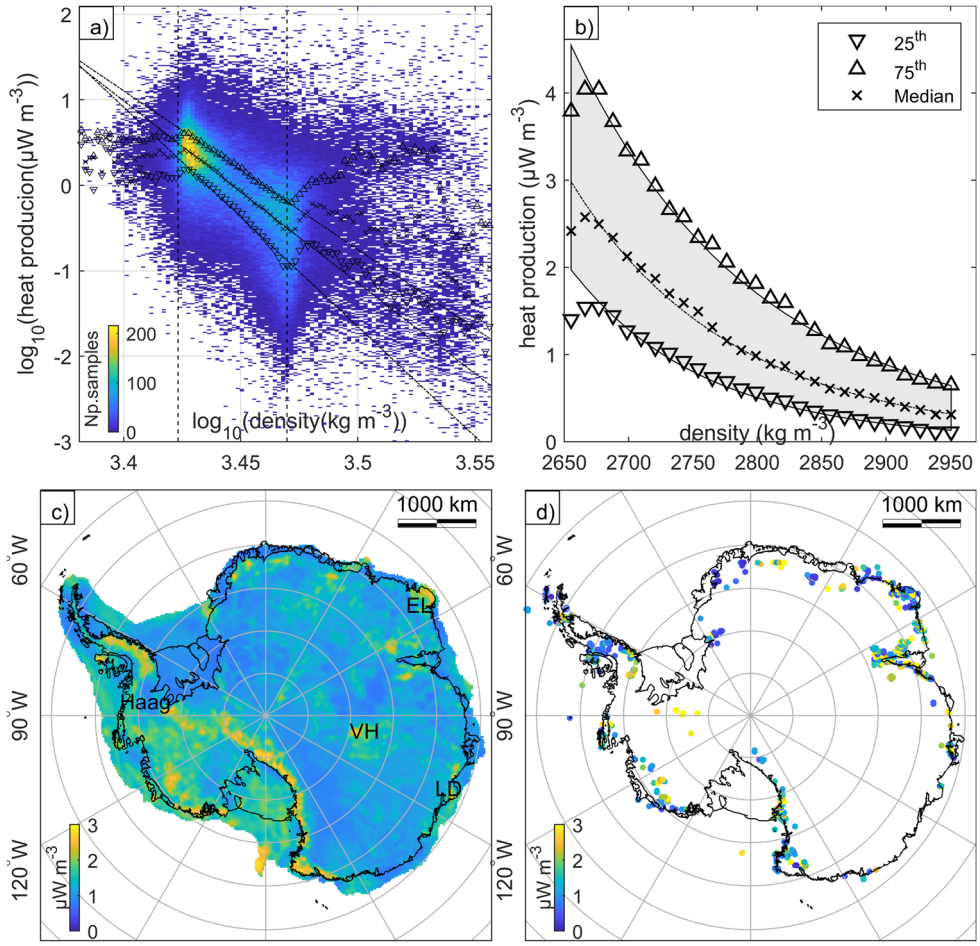

Figure 1. Estimation of radiogenic heat production in Antarctica. (a) 2D histogram shows empirical density and heat production relationship in $\log_{10}$ space using a global data set (Gard et al., 2019a). The upper and lower triangles, and the cross, represent the 75th, 25th, and median heat production values in each density bin, respectively. The dash-dotted line indicates the linear regression; (b) linear regression of density and heat production, with the density extension is set with the dashed-line range in panel (a); (c) modeled heat production map based on the empirical relationship using median density-heat production relationship; (d) median heat production value from PetroChron Antarctica data set in 20 × 20 km cell bin. It shows spatially limited heat production estimates based on geological samples across Antarctica (Sanchez et al., 2021). EL, Enderby Land; LD, Law Dome; VH, Vostok Highland. Colormap is truncated at 3 μW/m^3.

(R^2 = 0.993), which captures most igneous and metamorphic rocks. A similar relationship is evident for the 25th and 75th percentiles of the data set. Therefore, for a given density, we can estimate the most central heat production value in the global database and the associated interquartile range. Although the potential exists for systemic biases in the global geochemical database or anomalous crust in parts of Antarctica, we suggest that the density-heat production trends for large rock volumes should sit within the boundaries of the globally defined relationship.

3. Results

3.1. Antarctic Crustal Structure

Our model-ensemble results indicate spatial variations in sedimentary layer thickness beneath the ice sheet and ice shelf (Figure 2a and Figure S6a in Supporting Information S1). We have resolved a sedimentary layer with average 1 km thickness in onshore West Antarctica where sedimentary basin is present. These results are consistent with passive seismic estimations (Chaput et al., 2014; Dunham et al., 2020; Zhou et al., 2022). In contrast, the East Antarctica section preserves thicker sedimentary packages, with an average thickness of 2 km.

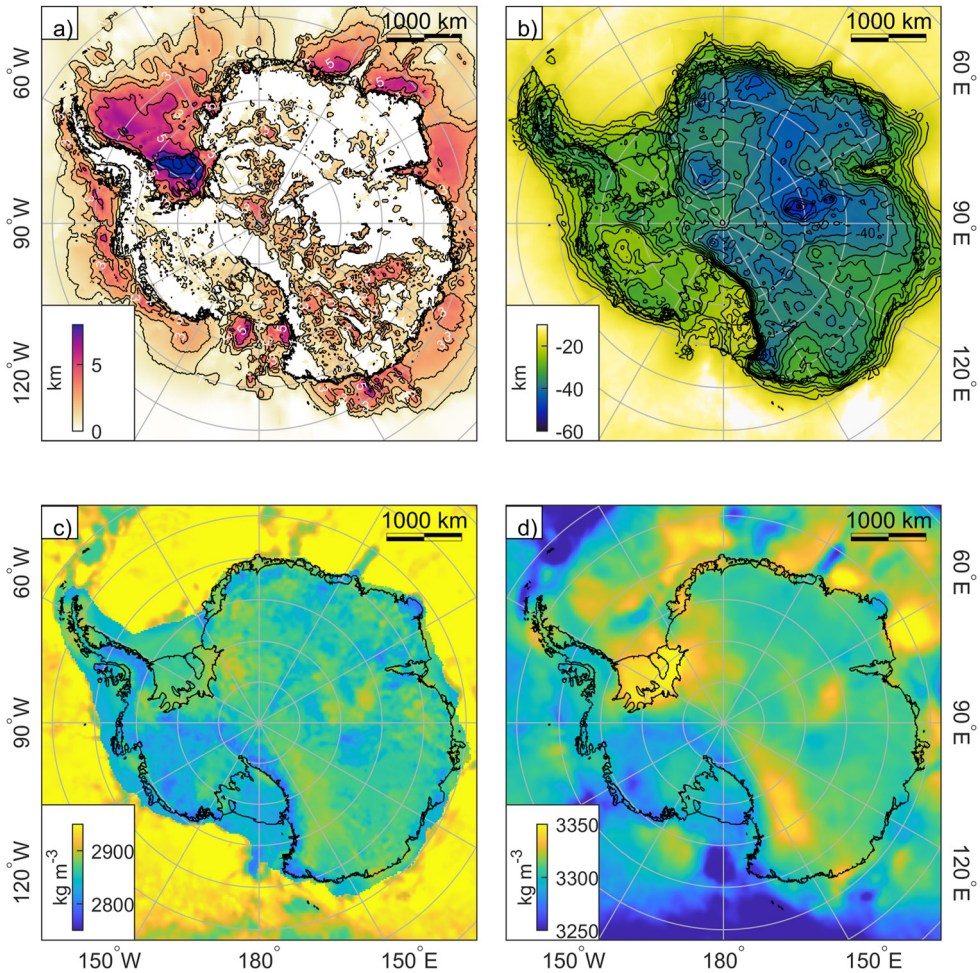

Figure 2. The estimated structures from model-ensemble mean includes: (a) sedimentary basin thickness; (b) Moho depth; (c) crystalline crust density; and (d) mantle density. The model suggests distinct structures when comparing East Antarctica (thick basin, thick and dense crust) with West Antarctica (thin basin, thin and less dense crust), and highlights small-scale variations within the crust.

Major and thick sedimentary basins (3–4 km) are preserved in the Aurora Subglacial Basin and Pensacola Pole Basin. The Wilkes Subglacial Basin is thinner (1–2 km) in the north, with a thicker basin in the south (3–4 km). Thick sedimentary basins are identified beneath major ice shelves, with a thickness of 8–12 km resolved in the Filchner-Ronne Ice Shelf (FRIS). The basin is thickest closest to the edge of the ice shelf and becomes thinner toward the western side of the inner ice shelf. For the Ross Ice Shelf (RIS), we have resolved near 1–3 km of sediment that is thicker from the grounding line to the edge of the ice shelf into the Ross Sea. The western side of the RIS is generally thicker than the eastern side, separated by a mid-shelf high (Tankersley et al., 2022). The sedimentary basin beneath the Amery Ice Shelf is narrower, with a thickness of 3 km.

The thinner crust in West Antarctica (25 km) and thicker crust in East Antarctica (35 km) are captured by the mean Moho as shown in Figure 2b and Figure S6b in Supporting Information S1. The thinnest crust occurs in the Ross Sea, Byrd Subglacial Basin, and Byrd Subglacial Trench as part of the West Antarctic Rift System (WARS), while the thickest crust occurs beneath the Gamburtsev Subglacial Mountains (GSM). The standard deviation of the Moho surface shows variability within the model-ensemble, as seen in Figure S6 in Supporting Information S1. This variability reflects both the consistency of the initial model with the gravity field and the influence of the applied constraints. High standard deviation occurs where constraints are weak, and the initial model does not explain gravity observations. Conversely, low standard deviation occurs where either constraint is strong or the initial model is already explaining gravity observations. For instance, in the GSM region, we see that the deep Moho, constrained by seismic data (Hansen et al., 2010) shows a large variance after inversion. This large Moho

variation indicates that the initial Moho does not match gravity observation, which requires either reducing the crust thickness (Pappa et al., 2019a) or including a dense mafic underplate structure (Ferraccioli et al., 2011). In the Wilkes Land region, the Moho shows low variance despite low seismic data constraints. This indicates that the initial isostatic assumption is close to matching the gravity observation.

3.2. Antarctic Crustal Heat Production Estimate

Applying the empirical density to heat production relationship to our modeled upper-crust density, we generated an upper-crust heat production map (Figure 1c). The map shows that West Antarctica generally has expected heat production higher than in East Antarctica, with broad areas exhibiting expected heat production higher than 1.8 $\mu W/m^3$, except for the ridge of the WARS and the Haag block with expected heat production less than 1.4 $\mu W/m^3$. East Antarctica shows lower expected heat production, with an average of 1.2 $\mu W/m^3$, while local areas such as Law Dome, Enderby Land, Vostok Highland, and the Dronning Maud Land (DML) region have expected heat production higher than 2 $\mu W/m^3$. On the other hand, GSM and the southern Wilkes Subglacial Basin exhibit low expected heat production, less than 1 $\mu W/m^3$.

4. Discussion

4.1. Model Limitations and Value

At continental-scale, gravity inversion has low sensitivity to the depth of anomaly sources. Residual gravity anomalies longer than 400 km in wavelength (five times model vertical extension) are effectively indistinguishable from a 1D response, meaning that the depth of the sources of these anomalies is undefined. The low vertical sensitivity might account for the similar structure observed for both the mantle and crustal density. Our model sensitivity test indicates that, given the current constraints, changing the mantle density alone is insufficient to account for the residual gravity anomaly (Figure S4a in Supporting Information S1). On the other hand, crustal density has the power necessary to explain all onshore residual gravity anomalies (Figure S4c in Supporting Information S1). In this situation, the crustal anomaly could be up to 50% greater than the model-ensemble mean. However, a homogenous mantle is unlikely where seismic tomography models reveal large lateral variations in the upper mantle (An et al., 2015a; Lloyd et al., 2020; Shen et al., 2018).

The most robust constraint in our model is the Moho measurement. The model-ensemble mean Moho depth is close to the seismic Moho estimations with an RMS misfit of 3.8 km. This misfit falls within the uncertainty range of 3–5 km from receiver function studies (Figure S7 in Supporting Information S1), which is lower than the RMS misfit of other continental-scale models (e.g., 6.9 km in Pappa et al. (2019b), 6.2 km in Zhang et al. (2020)). Although constraints do not exist for the density distribution in the crust and mantle, the mantle density derived from model-ensemble mean exhibits a similar structure to the average mantle Versus (50 km beneath Moho) obtained from Bayesian inversion of Rayleigh wave and receiver functions (Shen et al., 2018).

Several models exist that resolve the large-scale variations of crustal structure (Afonso et al., 2019; Haeger & Kaban, 2019; Laske et al., 2013), and also the situation for focused regions (Capponi et al., 2022; Lösing et al., 2022), but these models cannot connect the finer-scale variations with the larger scale variations across the continent as showed in our model.

4.2. GHF Due To Variable Heat Production

4.2.1. Heat Production Model Validation

A continental-scale heat production map had previously been estimated using inferred geological age and sparse outcrop (Stål et al., 2020). Due to the challenge of direct sampling from the subglacial environment, the geological age is largely unknown beneath the ice-sheet. Thus, in absence of ground-truth information in continental-scale, we compared our heat production map with the PetroChron Antarctica data set (Sanchez et al. (2021), Figure 1d), which is a geochemical estimation using outcrops. Our model shows a good match with the spatial distribution of heat production from the database, with elevated heat production in areas such as Antarctica Peninsula, TAM, Enderby Land, and Lambert Rift captured by our model. Our model also indicates low heat production values in the coastal region of East Antarctica. For a quantitative analysis, the misfit between the modeled heat production

is presented in the Figure S11 in Supporting Information S1 (mean = −0.14 μW/m^3, median = 0.26 μW/m^3, standard deviation = 1.67 μW/m^3). Despite a general concordance, significant misfits are seen between our expected heat production values and those calculated from PetroChron Antarctica, due to the difference in both sampled volumes and sampling frequency.

The opportunity remains for parts of Antarctica to be anomalous with respect to their relationship between crustal density and heat production. East Antarctica includes several regions known to have extensive Archean crust including in DML and Enderby Land (Cox et al., 2023), as well as regions with high-grade metamorphic rocks, including eclogites (Brown et al., 2020) and high-heat-producing granite suites (Carson et al., 2014). West Antarctica meanwhile has regions with active subduction zones as well as volcanism and underlying plutonism (Jordan et al., 2020). These regions and their subglacial counterparts may exhibit atypical density-heat production relationships that may exacerbate or moderate the variability defined by our model, however, it is not possible reliably to express these relationships from currently available data.

4.2.2. Implication for Radiogenic Crust Contribution for GHF

We calculated the contribution of radiogenic heat production from the crust to the total GHF by using the estimated heat production value (Figure 3c) and the upper-crust thickness (Figure 3b). Our findings suggest that radiogenic heat production could contribute up to 50 mW/m^2 to GHF. Areas with thick crust and high heat production show a greater crustal contribution. In specific regions such as Lambert, DML, and Vostok Highlands, the crustal heat production could contribute to GHF exceeding 40 mW/m^2 (Figure 3c). Our map also highlights higher heat production values in West Antarctica. However, due to the thin crust in West Antarctica, the crustal contribution from this region averages 20 mW/m^2. In some localized areas like the Antarctic Peninsula, Marie Byrd Land, and Ellsworth-Whitworth Mountains, the contribution from crustal heat production can be as high as 50 mW/m^2.

In Antarctica, continental-scale GHF estimation usually assumes a laterally uniform crustal heat production value (e.g., 1 μW/m^3 at the upper-crust (An et al., 2015b), or 2.5 μW/m^3 at the surface and exponentially decreasing to 8 km (Martos et al., 2017)). To illustrate the contribution of the spatially variable heat production to the total GHF, we use a uniform 1 μW/m^3 as a reference heat flow model for comparison. We calculate the radiogenic crust heat flow contribution with a minimum (25th percentile), median (Figure 3c), and maximum heat production case (75th percentile). We then compare our model results with the reference model (1 μW/m^3). All models are calculated with the same upper-crust thickness (Figure 3b).

The heat flow variation compared to the reference model is within 10 mW/m^2 for the most conservative heat production estimation (25th percentile fitting), with East Antarctica showing negative variation and West Antarctica a positive heat flow variation (Figure 3f). For the median case, the heat flow change compared with the reference model is mostly positive, with an increase of 0.6 mW/m^2 at the 25th percentile and 6.8 mW/m^2 at the 75th percentile. For the maximum heat production case (75th percentile fitting, Figure 3e), areas including Antarctica Peninsula, Marie Byrd Land, TA, and the DML area show a positive heat flow variation up to 50 mW/m^2 above the reference.

Although our model exhibits significant variability depending on the chosen scenario, it is evident that, in all cases, highly variable heat flux is expected to be derived from radiogenic crust heat production variation. Further testing, which consider the uncertainties of resolved density structure, reveals a similar pattern for elevated heat flow variation (Figure S12 in Supporting Information S1).

4.2.3. Implication for Ice Sheet System

GHF is a key boundary condition of the ice sheet flow as elevated heat flow warms the ice sheet bed, affecting ice rheology and potentially increasing basal melt rate (McCormack et al., 2022). Regions with higher GHF also lead to the formation of temperate ice, which in turn results in faster surface flow (Pittard et al., 2016). GHF also impacts ice sheet dynamic related subglacial hydrology. In areas where the basal temperature exceeds the pressure melting point, subglacial meltwater is generated, forming an input to the hydrological system. Based on numerical ice sheet modeling, the basal melting rate increases linearly with GHF at a rate of approximately 0.1–0.4 mm/yr/(mW/m^2) (Joughin et al., 2009; Seroussi et al., 2017).

When considering the contribution of heat production to GHF, the model suggests a strong spatial variation in heat flow (ranging from 6 to 60 mW/m^2) due to the incorporation of variations in crustal heat production. Considering

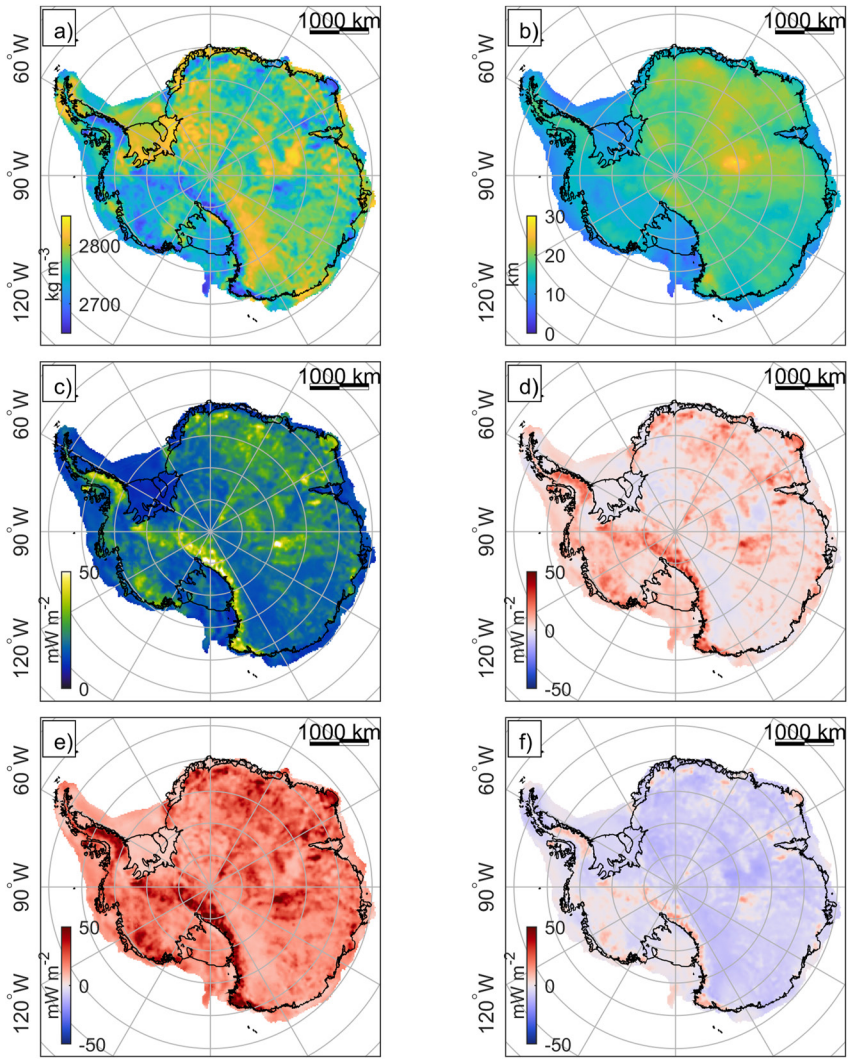

Figure 3. GHF contribution from upper-crust heat production using empirical density-heat production relationship. (a) upper-crust density; (b) upper-crust thickness; (c) heat flow contribution due to crust heat production (median fitting, 16–24 mW/m^2 from 25th to 75th percentile); (d) heat flow variation (median fitting) compared to uniform upper-crust heat production at reference value (1 μW/m^3); (e) heat flow variation (75th percentile fitting) compared to uniform upper-crust heat production; (f) heat flow variation (25th percentile fitting) compared to uniform upper-crust heat production.

that mantle heat flow contributes to a long-wavelength heat source beneath the ice sheet, the short-wavelength heat source resolved by our model (40 km) resulting from crustal heat production could result in a spatially heterogeneous basal melt (0.6–24 mm/yr). This spatial variability in basal conditions could be a crucial factor for the subglacial hydrology system and impact ice sheet dynamics.

5. Conclusions

We developed a model-ensemble of the crustal structure of Antarctica using gravity inversion, constrained by seismic information. Analyzing the resulting upper-crustal density we estimated expected volumetric heat production using an empirical relationship defined from a global geochemical database on the basis that the rock-volumes represented in our model elements are overall consistent with the global sample set. Incorporating also upper-crust thickness, we generated a continental-scale crustal radiogenic heat production estimation and its contribution to spatially variable GHF (ranging from 6 to 60 mW/m^2).

Our work offers crucial insights into the likely pattern and magnitude of heterogeneity in a key heat source beneath the ice sheet, and associated limits. The identified crustal heterogeneity and its uncertainties are key to

bridging regional heat flow models with the small-scale resolutions necessary to improve our understanding of ice sheet dynamics. By integrating these models with additional constraints from other geophysical measurements, we can update and refine the statistical estimation of GHF for Antarctica.

Data Availability Statement

The model of Antarctic crustal structure and radiogenic heat production is available in Zenodo repository (Li & Aitken, 2023a) and code for generate figure and radiogenic heat production is available in Li and Aitken (2023b).

Acknowledgments
This research was supported by the Australian Research Council Special Research Initiative, Australian Centre for Excellence in Antarctic Science (SR200100008). L.L. was supported by China Scholarship Council–The University of Western Australia joint PhD scholarship (201806170054). We thank editor Daoyuan Sun for handling our work and insightful reviews from Jörg Ebbing, Judith Freienstein and Tobias Stål to great improve the manuscript. We also thank Kirsty Tinto for her constructive comments on an earlier version of the manuscript. Open access publishing facilitated by The University of Western Australia, as part of the Wiley—The University of Western Australia agreement via the Council of Australian University Librarians.

References

Abrehdary, M., & Sjöberg, L. (2021). Moho density contrast in Antarctica determined by satellite gravity and seismic models. *Geophysical Journal International*, *225*(3), 1952–1962. https://doi.org/10.1093/gji/ggab069

Afonso, J. C., Salajegheh, F., Gaina, C., Ebbing, J., & Szwillus, W. (2019). A global reference model of the lithosphere and upper mantle from joint inversion and analysis of multiple data sets. *Geophysical Journal International*, *217*(3), 1602–1628. https://doi.org/10.1093/gji/ggz094

Aitken, A. (2010). Moho geometry gravity inversion experiment (MoGGIE): A refined model of the Australian Moho, and its tectonic and isostatic implications. *Earth and Planetary Science Letters*, *297*(1–2), 71–83. https://doi.org/10.1016/j.epsl.2010.06.004

Aitken, A., Salmon, M., & Kennett, B. (2013). Australia's Moho: A test of the usefulness of gravity modelling for the determination of Moho depth. *Tectonophysics*, *609*, 468–479. https://doi.org/10.1016/j.tecto.2012.06.049

Alghamdi, A., Aitken, A., & Dentith, M. (2018). The deep crustal structure of the Warakurna LIP, and insights on Proterozoic LIP processes and mineralisation. *Gondwana Research*, *56*, 1–11. https://doi.org/10.1016/j.gr.2017.12.001

An, M., Wiens, D. A., Zhao, Y., Feng, M., Nyblade, A. A., Kanao, M., et al. (2015a). S-velocity model and inferred Moho topography beneath the Antarctic Plate from Rayleigh waves. *Journal of Geophysical Research: Solid Earth*, *120*(1), 359–383. https://doi.org/10.1002/2014jb011332

An, M., Wiens, D. A., Zhao, Y., Feng, M., Nyblade, A. A., Kanao, M., et al. (2015b). Temperature, lithosphere-asthenosphere boundary, and heat flux beneath the Antarctic Plate inferred from seismic velocities. *Journal of Geophysical Research: Solid Earth*, *120*(12), 8720–8742. https://doi.org/10.1002/2015jb011917

Baranov, A., & Morelli, A. (2013). The Moho depth map of the Antarctica region. *Tectonophysics*, *609*, 299–313. https://doi.org/10.1016/j.tecto.2012.12.023

Bell, R. E. (2008). The role of subglacial water in ice-sheet mass balance. *Nature Geoscience*, *1*(5), 297–304. https://doi.org/10.1038/ngeo186

Brown, D. A., Hand, M., Morrissey, L. J., & Goodge, J. W. (2020). Cambrian eclogite-facies metamorphism in the central Transantarctic Mountains, East Antarctica: Extending the record of early Palaeozoic high-pressure metamorphism along the eastern Gondwanan margin. *Lithos*, *366*, 105571. https://doi.org/10.1016/j.lithos.2020.105571

Burton-Johnson, A., Dziadek, R., & Martin, C. (2020). Geothermal heat flow in Antarctica: Current and future directions. *The Cryosphere*, *14*(11), 3843–3873. https://doi.org/10.5194/tc-14-3843-2020

Capponi, M., Sampietro, D., Ebbing, J., & Ferraccioli, F. (2022). Antarctica 3-D crustal structure investigation by means of the Bayesian gravity inversion: The Wilkes Land case study. *Geophysical Journal International*, *229*(3), 2147–2161. https://doi.org/10.1093/gji/ggac036

Carson, C. J., McLaren, S., Roberts, J. L., Boger, S. D., & Blankenship, D. D. (2014). Hot rocks in a cold place: High sub-glacial heat flow in East Antarctica. *Journal of the Geological Society*, *171*(1), 9–12. https://doi.org/10.1144/jgs2013-030

Chaput, J., Aster, R. C., Huerta, A., Sun, X., Lloyd, A., Wiens, D., et al. (2014). The crustal thickness of West Antarctica. *Journal of Geophysical Research: Solid Earth*, *119*(1), 378–395. https://doi.org/10.1002/2013jb010642

Chisenga, C., Yan, J., & Yan, P. (2019). A crustal thickness model of Antarctica calculated in spherical approximation from satellite gravimetric data. *Geophysical Journal International*, *218*(1), 388–400. https://doi.org/10.1093/gji/ggz154

Cox, S. C., Smith Lyttle, B., Elkind, S., Smith Siddoway, C., Morin, P., Capponi, G., et al. (2023). A continent-wide detailed geological map dataset of Antarctica. *Scientific Data*, *10*(1), 250. https://doi.org/10.1038/s41597-023-02152-9

Dunham, C., O'Donnell, J., Stuart, G., Brisbourne, A., Rost, S., Jordan, T., et al. (2020). A joint inversion of receiver function and Rayleigh wave phase velocity dispersion data to estimate crustal structure in West Antarctica. *Geophysical Journal International*, *223*(3), 1644–1657. https://doi.org/10.1093/gji/ggaa398

Ferraccioli, F., Finn, C. A., Jordan, T. A., Bell, R. E., Anderson, L. M., & Damaske, D. (2011). East Antarctic rifting triggers uplift of the Gamburtsev Mountains. *Nature*, *479*(7373), 388–392. https://doi.org/10.1038/nature10566

Fullagar, P. K., Pears, G. A., & McMonnies, B. (2008). Constrained inversion of geologic surfaces—Pushing the boundaries. *The Leading Edge*, *27*(1), 98–105. https://doi.org/10.1190/1.2831686

Gard, M., Hasterok, D., & Halpin, J. (2019a). Global whole-rock geochemical database compilation. *Earth System Science Data*, *11*(4), 1553–1566. https://doi.org/10.5194/essd-11-1553-2019

Gard, M., Hasterok, D., Hand, M., & Cox, G. (2019b). Variations in continental heat production from 4 Ga to the present: Evidence from geochemical data. *Lithos*, *342*, 391–406. https://doi.org/10.1016/j.lithos.2019.05.034

Haeger, C., & Kaban, M. K. (2019). Decompensative gravity anomalies reveal the structure of the upper crust of Antarctica. *Pure and Applied Geophysics*, *176*(10), 4401–4414. https://doi.org/10.1007/s00024-019-02212-5

Haeger, C., Kaban, M. K., Tesauro, M., Petrunin, A. G., & Mooney, W. D. (2019). 3D density, thermal and compositional model of the Antarctic lithosphere and implications for its evolution. *Geochemistry, Geophysics, Geosystems*, *0*(2), 688–707. https://doi.org/10.1029/2018GC008033

Haeger, C., Petrunin, A. G., & Kaban, M. K. (2022). Geothermal heat flow and thermal structure of the Antarctic lithosphere. *Geochemistry, Geophysics, Geosystems*, *23*(10), e2022GC010501. https://doi.org/10.1029/2022gc010501

Hansen, S. E., Julià, J., Nyblade, A. A., Pyle, M. L., Wiens, D. A., & Anandakrishnan, S. (2009). Using S wave receiver functions to estimate crustal structure beneath ice sheets: An application to the Transantarctic Mountains and East Antarctic craton. *Geochemistry, Geophysics, Geosystems*, *10*(8), Q08014. https://doi.org/10.1029/2009gc002576

Hansen, S. E., Nyblade, A. A., Heeszel, D. S., Wiens, D. A., Shore, P., & Kanao, M. (2010). Crustal structure of the Gamburtsev Mountains, East Antarctica, from S-wave receiver functions and Rayleigh wave phase velocities. *Earth and Planetary Science Letters*, *300*(3–4), 395–401. https://doi.org/10.1016/j.epsl.2010.10.022

Hasterok, D., & Chapman, D. S. (2007). Continental thermal isostasy: 2. Application to North America. *Journal of Geophysical Research*, *112*(B6), B06415. https://doi.org/10.1029/2006jb004664

Hasterok, D., & Chapman, D. S. (2011). Heat production and geotherms for the continental lithosphere. *Earth and Planetary Science Letters*, *307*(1–2), 59–70. https://doi.org/10.1016/j.epsl.2011.04.034

Hasterok, D., & Webb, J. (2017). On the radiogenic heat production of igneous rocks. *Geoscience Frontiers*, *8*(5), 919–940. https://doi.org/10.1016/j.gsf.2017.03.006

Hazzard, J. A. N., Richards, F. D., Goes, S. D. B., & Roberts, G. G. (2023). Probabilistic assessment of Antarctic thermomechanical structure: Impacts on ice sheet stability. *Journal of Geophysical Research: Solid Earth*, *128*(5), e2023JB026653. https://doi.org/10.1029/2023jb026653

Hooke, R. L. (2019). *Principles of glacier mechanics*. Cambridge university press.

Jordan, T. A., Riley, T. R., & Siddoway, C. S. (2020). The geological history and evolution of West Antarctica. *Nature Reviews Earth & Environment*, *1*(2), 117–133. https://doi.org/10.1038/s43017-019-0013-6

Joughin, I., Tulaczyk, S., Bamber, J. L., Blankenship, D., Holt, J. W., Scambos, T., & Vaughan, D. G. (2009). Basal conditions for Pine Island and Thwaites Glaciers, West Antarctica, determined using satellite and airborne data. *Journal of Glaciology*, *55*(190), 245–257. https://doi.org/10.3189/002214309788608705

Kvas, A., Mayer-Gürr, T., Krauss, S., Brockmann, J. M., Schubert, T. S., Schuh, W. D., Pail, R. G., et al. (2019). The satellite-only gravity field model GOCO06s. https://doi.org/10.5880/ICGEM.2019.002

Laske, G., Masters, G., Ma, Z., & Pasyanos, M. (2013). Update on CRUST1. 0—A 1-degree global model of Earth's crust. *Geophysical Research Abstracts*.

Li, L., & Aitken, A. (2023a). Antarctic crustal Model and radiogenic heat production [Dataset]. Zenodo. https://doi.org/10.5281/zenodo.10242299

Li, L., & Aitken, A. (2023b). Source code for ANT_Crust and radiogenic heat production (v1.0) [Software]. *Zenodo*. https://doi.org/10.5281/zenodo.10275112

Li, L., Aitken, A. R., Lindsay, M. D., & Kulessa, B. (2022). Sedimentary basins reduce stability of Antarctic ice streams through groundwater feedbacks. *Nature Geoscience*, *15*(8), 645–650. https://doi.org/10.1038/s41561-022-00992-5

Lloyd, A. J., Wiens, D. A., Zhu, H., Tromp, J., Nyblade, A. A., Aster, R. C., et al. (2020). Seismic structure of the Antarctic upper mantle imaged with adjoint tomography. *Journal of Geophysical Research: Solid Earth*, *125*(3). https://doi.org/10.1029/2019jb017823

Llubes, M., Seoane, L., Bruinsma, S., & Rémy, F. (2018). Crustal thickness of Antarctica estimated using data from gravimetric satellites. *Solid Earth*, *9*(2), 457–467. https://doi.org/10.5194/se-9-457-2018

Lösing, M., & Ebbing, J. (2021). Predicting geothermal heat flow in Antarctica with a machine learning approach. *Journal of Geophysical Research: Solid Earth*, *126*(6), e2020JB021499. https://doi.org/10.1029/2020jb021499

Lösing, M., Ebbing, J., & Szwillus, W. (2020). Geothermal heat flux in Antarctica: Assessing models and observations by Bayesian inversion. *Frontiers in Earth Science*, *8*, 105. https://doi.org/10.3389/feart.2020.00105

Lösing, M., Moorkamp, M., & Ebbing, J. (2022). Joint inversion based on variation of information—A crustal model of Wilkes Land, East Antarctica. *Geophysical Journal International*, *232*(1), 162–175. https://doi.org/10.1093/gji/ggac334

Martos, Y. M., Catalán, M., Jordan, T. A., Golynsky, A., Golynsky, D., Eagles, G., & Vaughan, D. G. (2017). Heat flux distribution of Antarctica unveiled. *Geophysical Research Letters*, *44*(22), 11417–11426. https://doi.org/10.1002/2017gl075609

McCormack, F. S., Roberts, J. L., Dow, C. F., Stål, T., Halpin, J. A., Reading, A. M., & Siegert, M. J. (2022). Fine-scale geothermal heat flow in Antarctica can increase simulated subglacial melt estimates. *Geophysical Research Letters*, *49*(15), e2022GL098539. https://doi.org/10.1029/2022gl098539

Morlighem, M., Rignot, E., Binder, T., Blankenship, D., Drews, R., Eagles, G., et al. (2020). Deep glacial troughs and stabilizing ridges unveiled beneath the margins of the Antarctic ice sheet. *Nature Geoscience*, *13*(2), 132–137. https://doi.org/10.1038/s41561-019-0510-8

Moro, P. D. S., Aitken, A. R. A., Giraud, J., Jessell, M. W., & Kohan Pour, F. (2023). Seismically constrained gravity inversions reveal magmatic and metamorphic processes at a major lithospheric boundary in northwestern Australia. *Tectonophysics*, *863*. 230003. https://doi.org/10.1016/j.tecto.2023.230003

Noble, T. L., Rohling, E. J., Aitken, A. R. A., Bostock, H. C., Chase, Z., Gomez, N., et al. (2020). The sensitivity of the Antarctic ice sheet to a changing climate: Past, present, and future. *Reviews of Geophysics*, *58*(4), e2019RG000663. https://doi.org/10.1029/2019RG000663

Pappa, F., Ebbing, J., & Ferraccioli, F. (2019a). Moho depths of Antarctica: Comparison of seismic, gravity, and isostatic results. *Geochemistry, Geophysics, Geosystems*, *20*(3), 1629–1645. https://doi.org/10.1029/2018gc008111

Pappa, F., Ebbing, J., Ferraccioli, F., & van der Wal, W. (2019b). Modeling satellite gravity gradient data to derive density, temperature, and viscosity structure of the Antarctic lithosphere. *Journal of Geophysical Research: Solid Earth*, *124*(11), 12053–12076. https://doi.org/10.1029/2019jb017997

Pittard, M., Roberts, J., Galton-Fenzi, B., & Watson, C. (2016). Sensitivity of the Lambert-Amery glacial system to geothermal heat flux. *Annals of Glaciology*, *57*(73), 56–68. https://doi.org/10.1017/aog.2016.26

Reading, A. M., Stål, T., Halpin, J. A., Lösing, M., Ebbing, J., Shen, W., et al. (2022). Antarctic geothermal heat flow and its implications for tectonics and ice sheets. *Nature Reviews Earth & Environment*, *3*(12), 814–831. https://doi.org/10.1038/s43017-022-00348-y

Sanchez, G., Halpin, J. A., Gard, M., Hasterok, D., Staal, T., Raimondo, T., et al. (2021). PetroChron Antarctica: A geological database for interdisciplinary use. *Geochemistry, Geophysics, Geosystems*, *22*(12), e2021GC010154. https://doi.org/10.1029/2021gc010154

Scheinert, M., Ferraccioli, F., Schwabe, J., Bell, R., Studinger, M., Damaske, D., et al. (2016). New Antarctic gravity anomaly grid for enhanced geodetic and geophysical studies in Antarctica. *Geophysical Research Letters*, *43*(2), 600–610. https://doi.org/10.1002/2015GL067439

Seroussi, H., Ivins, E. R., Wiens, D. A., & Bondzio, J. (2017). Influence of a West Antarctic mantle plume on ice sheet basal conditions. *Journal of Geophysical Research: Solid Earth*, *122*(9), 7127–7155. https://doi.org/10.1002/2017jb014423

Shen, W., Wiens, D., Anandakrishnan, S., Aster, R., Gerstoft, P., Bromirski, P., et al. (2018). The crust and upper mantle structure of central and west Antarctica from Bayesian inversion of Rayleigh wave and receiver functions. *Journal of Geophysical Research-Solid Earth*, *123*(9), 7824–7849. https://doi.org/10.1029/2017jb015346

Stål, T., Reading, A. M., Halpin, J. A., Phipps, S. J., & Whittaker, J. M. (2020). The Antarctic crust and upper mantle: A flexible 3D model and software framework for interdisciplinary research. *Frontiers in Earth Science*, *8*, 1–19. https://doi.org/10.3389/feart.2020.577502

Stål, T., Reading, A. M., Halpin, J. A., & Whittaker, J. M. (2019). A multivariate approach for mapping lithospheric domain boundaries in East Antarctica. *Geophysical Research Letters*, *46*(17–18), 10404–10416. https://doi.org/10.1029/2019gl083453

Stål, T., Reading, A. M., Halpin, J. A., & Whittaker, J. M. (2021). Antarctic geothermal heat flow model: Aq1. *Geochemistry, Geophysics, Geosystems*, *22*(2), e2020GC009428. https://doi.org/10.1029/2020gc009428

Tankersley, M. D., Horgan, H. J., Siddoway, C. S., Tontini, F. C., & Tinto, K. J. (2022). Basement topography and sediment thickness beneath Antarctica's Ross Ice Shelf. *Geophysical Research Letters*, *49*(10), e2021GL097371. https://doi.org/10.1029/2021gl097371

Zhang, C., von Frese, R. R., Shum, C., Leftwich, T. E., Kim, H. R., & Golynsky, A. V. (2020). Satellite gravity constraints on the Antarctic Moho and its potential isostatic adjustments. *Geochemistry, Geophysics, Geosystems*, *21*(12), e2020GC009048. https://doi.org/10.1029/2020gc009048

Zhou, Z., Wiens, D. A., Shen, W., Aster, R. C., Nyblade, A., & Wilson, T. J. (2022). Radial Anisotropy and sediment thickness of West and Central Antarctica estimated from Rayleigh and Love wave velocities. *Journal of Geophysical Research: Solid Earth*, *127*(3), e2021JB022857. https://doi.org/10.1029/2021jb022857

References From the Supporting Information

Agostinetti, N. P., Amato, A., Cattaneo, M., & Di Bona, M. (2004). Crustal structure of northern Victoria Land from receiver function analysis. *Terra Antarctica*, *11*(1), 5–14.

Aitken, A. R., Roberts, J. L., van Ommen, T. D., Young, D. A., Golledge, N. R., Greenbaum, J. S., et al. (2016). Repeated large-scale retreat and advance of Totten Glacier indicated by inland bed erosion. *Nature*, *533*(7603), 385–389. https://doi.org/10.1038/nature17447

Aitken, A. R. A., Li, L., Kulessa, B., Schroeder, D., Jordan, T. A., Whittaker, J. M., et al. (2023). Antarctic sedimentary basins and their influence on ice-sheet dynamics. *Reviews of Geophysics*, *61*(3), e2021RG000767. https://doi.org/10.1029/2021RG000767

Bannister, S., Yu, J., Leitner, B., & Kennett, B. (2003). Variations in crustal structure across the transition from West to East Antarctica, Southern Victoria Land. *Geophysical Journal International*, *155*(3), 870–880. https://doi.org/10.1111/j.1365-246x.2003.02094.x

Bayer, B., Geissler, W. H., Eckstaller, A., & Jokat, W. (2009). Seismic imaging of the crust beneath Dronning Maud Land, East Antarctica. *Geophysical Journal International*, *178*(2), 860–876. https://doi.org/10.1111/j.1365-246x.2009.04196.x

Becker, D., Jordan, T., Corr, H., & Robinson, C. (2018). Strapdown aerogravity survey across the Brunt ice shelf, 2017. https://doi.org/10.5285/79e63097-f5dc-41ff-8ca5-36bc4f95a6ff

Burton-Johnson, A., Halpin, J., Whittaker, J. M., Graham, F. S., & Watson, S. J. (2017). A new heat flux model for the Antarctic Peninsula incorporating spatially variable upper crustal radiogenic heat production. *Geophysical Research Letters*, *44*(11), 5436–5446. https://doi.org/10.1002/2017gl073596

Eittreim, S. L. (1994). Transition from continental to oceanic crust on the Wilkes-Adélie margin of Antarctica. *Journal of Geophysical Research*, *99*(B12), 24189–24205. https://doi.org/10.1029/94jb01903

Feng, M., An, M., & An, C. (2014). Crustal thicknesses along the traverse from Zhongshan to Dome A in east Antarctica. *Chinese Journal of Polar Research*, *26*(2), 177–185.

Frederick, B. C., Young, D. A., Blankenship, D. D., Richter, T. G., Kempf, S. D., Ferraccioli, F., & Siegert, M. J. (2016). Distribution of subglacial sediments across the Wilkes Subglacial Basin, East Antarctica. *Journal of Geophysical Research: Earth Surface*, *121*(4), 790–813. https://doi.org/10.1002/2015JF003760

Gard, M., Hasterok, D., & Halpin, J. (2019). Global whole-rock geochemical database compilation. *Earth System Science Data*, *11*(4), 1553–1566. https://doi.org/10.5194/essd-11-1553-2019

Golynsky, A., Chiappini, M., Damaske, D., Ferraccioli, F., Finn, C. A., Ishihara, T., et al. (2006). ADMAP—A digital magnetic anomaly map of the Antarctic. In *Antarctica* (pp. 109–116). Springer.

Guterch, A., Grad, M., Janik, T., Perchuć, E., & Pajchel, J. (1985). Seismic studies of the crustal structure in West Antarctica 1979–1980—Preliminary results. *Tectonophysics*, *114*(1–4), 411–429. https://doi.org/10.1016/0040-1951(85)90024-1

Hasterok, D., Gard, M., & Webb, J. (2018). On the radiogenic heat production of metamorphic, igneous, and sedimentary rocks. *Geoscience Frontiers*, *9*(6), 1777–1794. https://doi.org/10.1016/j.gsf.2017.10.012

Hoffmann, M., Eckstaller, A., Jokat, W., & Miller, H. (2003). Development of a 3-D crustal model in the western Dronning Maud Land Region, Antarctica, from the interpretation of different geophysical data sets.

Hübscher, C., Jokat, W., & Miller, H. (1996). Structure and origin of southern Weddell Sea crust: Results and implications. *Geological Society, London, Special Publications*, *108*(1), 201–211. https://doi.org/10.1144/gsl.sp.1996.108.01.15

Hungelng, A., & Thyssen, F. (1991). Reflection seismic measurements in western Neuschwabenland. International symposium on Antarctic Earth sciences (Vol. *5*).

Ikami, A., & Ito, K. (1986). Crustal structure in the Mizuho Plateau, East Antarctica, by a two-dimensional ray approximation. *Journal of Geodynamics*, *6*(1–4), 271–283. https://doi.org/10.1016/0264-3707(86)90044-x

Isanina, E. V., Krupnova, N. A., Popov, S. V., Masolov, V. N., & Lukin, V. V. (2009). Deep structure of the Vostok Basin, East Antarctica as deduced from seismological observations. *Geotectonics*, *43*(3), 221–225. https://doi.org/10.1134/s0016852109030042

Jokat, W., Fechner, N., & Studinger, M. (1997). *The Antarctic region: Geological evolution and processes*. Terra Antarctica Publication.

Jokat, W., Ritzmann, O., Reichert, C., & Hinz, K. (2004). Deep crustal structure of the continental margin off the explora escarpment and in the Lazarev Sea, East Antarctica. *Marine Geophysical Researches*, *25*(3–4), 283–304. https://doi.org/10.1007/s11001-005-1337-9

Kanao, M. (2012). *Seismic waves: Research and analysis*. BoD–Books on Demand.

Kogan, A. L. (1974). Deep seismic sounding of the Earth's crust in East Antarctica. *Antarctica*, *3*, 85–104.

Kolmakov, A. F., Mishenkin, B. P., & Solovyev, D. S. (1975). Deep seismic studies in East Antarctica. *Bull Soviet Antarc Exped*, 5–15.

Kudryavtzev, G. A., Butzenko, V. V., & Kadmina, I. N. (1991). Crustal section across western Dronning Maud Land continental margin from geophysical data. Abstracts, Sixth international symposium on Antarctic earth science.

Lawrence, J. F., Wiens, D. A., Nyblade, A. A., Anandakrishnan, S., Shore, P. J., & Voigt, D. (2006a). Crust and upper mantle structure of the Transantarctic Mountains and surrounding regions from receiver functions, surface waves, and gravity: Implications for uplift models. *Geochemistry, Geophysics, Geosystems*, *7*(10), Q10011. https://doi.org/10.1029/2006gc001282

Lawrence, J. F., Wiens, D. A., Nyblade, A. A., Anandakrishnan, S., Shore, P. J., & Voigt, D. (2006b). Rayleigh wave phase velocity analysis of the Ross Sea, Transantarctic Mountains, and East Antarctica from a temporary seismograph array. *Journal of Geophysical Research*, *111*(B6), B06302. https://doi.org/10.1029/2005jb003812

Leitchenkov, G. L., & Kudryavtzev, G. (2000). Structure and origin of the Earth´s crust in the Weddell Sea embayment (beneath the front of the Filchner and Ronne ice shelves) from deep seismic sounding data. *Polarforschung*, *67*(3), 143–154.

Kanao, M., Kubo, A., Shibutani, T., Negishi, H., & Tono, Y. (2002). Crustal structure around the Antarctic margin by teleseismic receiver function analyses. In D. N. B. S. A. S. H. J. A. Gamble (Ed.), *Antarctica at the close of a millennium* (Vol. 35, pp. 485–491). Royal Society of New Zealand Bulletin.

Maritati, A., Aitken, A. R. A., Young, D. A., Roberts, J. L., Blankenship, D. D., & Siegert, M. J. (2016). The tectonic development and erosion of the Knox subglacial sedimentary basin, East Antarctica. *Geophysical Research Letters*, *43*(20), 10728–10737. https://doi.org/10.1002/2016gl071063

McGuiness, L. D., Bowen, R. H., Erichson, J. M., Allred, B. J., & Kreamer, J. L. (1985). East-West Antarctic boundary in McMurdo Sound. *Tectonophysics*, *114*(1–4), 341–356. https://doi.org/10.1016/0040-1951(85)90020-4

Miyamachi, H., Toda, S., Matsushima, T., Takada, M., Watanabe, A., Yamashita, M., & Kanao, M. (2003). Seismic refraction and wide-angle reflection exploration by JARE-43 on Mizuho Plateau, East Antarctica.

Pappa, F., Ebbing, J., & Ferraccioli, F. (2019). Moho depths of Antarctica: Comparison of seismic, gravity, and isostatic results. *Geochemistry, Geophysics, Geosystems*, *20*(3), 1629–1645. https://doi.org/10.1029/2018gc008111

Paxman, G. J., Jamieson, S. S., Ferraccioli, F., Jordan, T. A., Bentley, M. J., Ross, N., et al. (2019). Subglacial geology and geomorphology of the Pensacola-Pole basin, East Antarctica. *Geochemistry, Geophysics, Geosystems*, *20*(6), 2786–2807. https://doi.org/10.1029/2018GC008126

Piana Agostinetti, N., Roselli, P., Cattaneo, M., & Amato, A. (2005). *Moho-depth and subglacial sedimentary layer thickness in the Wilkes Basin from receiver function analysis*. IASPEI-General Assembly.

Ramirez, C., Nyblade, A., Emry, E. L., Julià, J., Sun, X., Anandakrishnan, S., et al. (2017). Crustal structure of the Transantarctic Mountains, Ellsworth Mountains and Marie Byrd Land, Antarctica: Constraints on shear wave velocities, Poisson's ratios and Moho depths. *Geophysical Journal International*, *211*(3), 1328–1340. https://doi.org/10.1093/gji/ggx333

Ramirez, C., Nyblade, A., Hansen, S., Wiens, D. A., Anandakrishnan, S., Aster, R. C., et al. (2016). Crustal and upper-mantle structure beneath ice-covered regions in Antarctica from S-wave receiver functions and implications for heat flow. *Geophysical Journal International*, *204*(3), 1636–1648. https://doi.org/10.1093/gji/ggv542

Reading, A. M. (2004). The seismic structure of Wilkes Land/Terre Adelie, East Antarctica and comparison with Australia: First steps in reconstructing the deep lithosphere of Gondwana. *Gondwana Research*, *7*(1), 21–30. https://doi.org/10.1016/s1342-937x(05)70303-8

Reading, A. M. (2006). The seismic structure of Precambrian and early Palaeozoic terranes in the Lambert Glacier region, East Antarctica. *Earth and Planetary Science Letters*, *244*(1–2), 44–57. https://doi.org/10.1016/j.epsl.2006.01.031

Rybach, L. (1988). Determination of heat production rate. In *Handbook of terrestrial heat flow density determination* (p. 486).

Sandwell, D. T., Muller, R. D., Smith, W. H. F., Garcia, E., & Francis, R. (2014). New global marine gravity model from CryoSat-2 and Jason-1 reveals buried tectonic structure. *Science*, *346*(6205), 65–67. https://doi.org/10.1126/science.1258213

Straume, E. O., Gaina, C., Medvedev, S., Hochmuth, K., Gohl, K., Whittaker, J. M., et al. (2019). GlobSed: Updated total sediment thickness in the world's oceans. *Geochemistry, Geophysics, Geosystems*, *20*(4), 1756–1772. https://doi.org/10.1029/2018gc008115

Studinger, M., Karner, G. D., Bell, R. E., Levin, V., Raymond, C. A., & Tikku, A. (2003). Geophysical models for the tectonic framework of the Lake Vostok region, East Antarctica. *Earth and Planetary Science Letters*, *216*(4), 663–677. https://doi.org/10.1016/s0012-821x(03)00548-x

Tinto, K. J., Padman, L., Siddoway, C. S., Springer, S. R., Fricker, H. A., Das, I., et al. (2019). Ross Ice Shelf response to climate driven by the tectonic imprint on seafloor bathymetry. *Nature Geoscience*, *12*(6), 441–449. https://doi.org/10.1038/s41561-019-0370-2

Trey, H., Cooper, A. K., Pellis, G., Della Vedova, B., Cochrane, G., Brancolini, G., & Makris, J. (1999). Transect across the West Antarctic Rift System in the Ross Sea, Antarctica. *Tectonophysics*, *301*(1–2), 61–74. https://doi.org/10.1016/s0040-1951(98)00155-3

Vuan, A., Brancolini, G., Panza, G. F., Russi, M., & Wu, F. (2001). Joint inversion of receiver function of teleseismic body waves and local group velocity dispersion curves beneath ESPZ and PMSA stations (Antarctic Peninsula). *Terra Antartica*, *8*(1–2), 49–54.

Winberry, J. P., & Anandakrishnan, S. (2004). Crustal structure of the West Antarctic Rift System and Marie Byrd Land hotspot. *Geology*, *32*(11), 977–980. https://doi.org/10.1130/g20768.1

Yoshii, K., Ito, K., Miyamachi, H., & Kanao, M. (2004). Crustal structure derived from seismic refractions and wide-angle reflections in the Mizuho Plateau, East Antarctica.

Young, D. A., Richter, T. G., Powell, E. M., Quartini, E., & Blankenship, D. D. (2017). Gravity disturbance data over central Marie Byrd Land, West Antarctica (GIMBLE.GGCMG2). https://doi.org/10.15784/601003